Optical model calculations for the elastic scattering of intermediate energy alpha particles

Anders Ingemarsson
The Svedberg Laboratory and Department of Radiation Sciences, Uppsala University, Box 533, S-75121 Uppsala, Sweden

Agris Auce and Roger Johansson
Department of Radiation Sciences, Uppsala University, Box 535, S-75121 Uppsala, Sweden

(Received 17 February 1993; revised manuscript received 14 October 1993)

Optical model calculations for intermediate energy alpha particles are performed with single-folded potentials using a Woods-Saxon parametrization for the matter densities and Gaussians for the effective alpha-nucleon interaction. A nearside and farside decomposition of the angular distributions are performed. We show that the refraction determines the gross features of the angular distributions.

PACS number(s): 24.10.Ht, 25.55.Ci

I. INTRODUCTION

Angular distributions of differential cross sections in the elastic scattering of alpha particles at energies below 100 MeV show typical diffractive patterns with well-defined sharp minima. From these minima it is possible to determine a Fraunhofer "strong absorption" radius. A strong absorption radius may also be defined from the S matrix or from the total reaction cross section, as discussed in the review article by Batty *et al.* [1]. This excellent article discusses many important features of alpha particle scattering. The great disadvantage with all these accurately determined strong absorption radii is the fact that they have no simple interpretation in terms of the matter densities.

When alpha particles of intermediate energies (>100 MeV) became available, it was found that the diffractive pattern in the angular cross section distribution was followed by an exponential falloff. Many analyses have shown that the large-angle behavior is very sensitive to the real part of the optical potential at very small radii. In a recent report [2], it was shown that the strong real potential of the alpha particles substantially reduces the absorption in the interior of the nucleus. This effect is an important reason why alpha particles can probe the interior of the nucleus.

Hussein and McVoy have shown [3] that a near-side and far-side decomposition of the differential cross section offers a possibility to get a much better insight into the strong sensitivity to the real potential in the elastic scattering of heavy ions and alpha particles. We will therefore do such a decomposition, following the method suggested by Fuller [4].

The aim of the calculations presented here was to learn more about the energy dependence of the interaction between alpha particles and nuclei. The motivation for this was the fact that we in the near future will perform a measurement of total reaction cross sections for alpha particles in the energy range 100–200 MeV. We have used a very simple single-folding model, and our ambition was not to obtain a perfect agreement with the experimental angular distributions, but to find systematic trends with energy.

II. ANALYSIS

The calculations were done with the code ECIS [5] using the folding model option. With this option the potentials are obtained from

$$U(r)=-\int [V(r')f(r-r')+iW(r')g(r-r')]d^3r' , \tag{1}$$

where $V(r')$ and $W(r')$ are Woods-Saxon potentials and $f(r-r')$ and $g(r-r')$ are Gaussian folding functions given by

$$f(r-r')=\frac{1}{(2\pi)^{3/2}\beta^3}e^{-(r-r')^2/\beta^2} . \tag{2}$$

Folding calculations for alpha particles and other particles are often performed using the same folding parameters β for the real and imaginary potentials. Sometimes, only the real potential is folded and the imaginary potential is assumed to have a Woods-Saxon shape. It is well known from optical model calculations, however, that much better fits can be obtained with different shapes of the real and imaginary potentials. Consequently, we decided to perform the folding with different folding parameters. We also considered it more meaningful to make comparisons between two folded potentials than between one folded and one of the conventional Woods-Saxon shape.

If the radial parameters of the two potentials are the same and equal to the parameters of the matter distribution, Eq. (1) is equivalent to a folding of the matter density with an effective interaction

$$U(r)=-\int \rho_m(r')V_{\text{eff}}(r,r')d^3r' , \tag{3}$$

where $\rho_m(r')$ is the matter density of the target nucleus and $V_{\text{eff}}(r,r')$ is the effective alpha-nucleon interaction. This interaction includes the effect of the finite size of the alpha particle. Therefore the β values are expected to be larger than 1 fm. Our effective interaction may be written as

$$f(q)=\frac{\sigma k}{4\pi}(ie^{-\beta_i^2q^2}+\alpha e^{-\beta_r^2q^2}) . \tag{4}$$

The quantities in this expression are related to the parameters of the optical potential by

$$\sigma = 2\mu\gamma_{\text{rel}} W/(kn_c) , \tag{5a}$$

$$\alpha = V/W , \tag{5b}$$

where μ is the reduced mass, k the wave number, and γ_{rel} the relativistic enhancement factor, which according to Ref. [6] is $k/(\mu v)$, were v is the velocity of the projectile in the laboratory system and n_c is the normalization factor of the matter distribution, which approximately is given by

$$n_c = \frac{4}{3}\pi R^3 \left[1 + \left[\frac{\pi a}{R}\right]^2\right] . \tag{6}$$

The analyses were done in the same phenomenological way as in optical model calculations. The matter distributions, well known from electron scattering and other experiments, were allowed to vary without any restrictions. The parameters of the interaction also varied freely. We will see below that this approach made it possible to draw important conclusions about the general features of elastic scattering of alpha particles.

The fitting procedure was done as a grid search for the real folding parameter β_r. For each value of β_r, we obtained the strength of the real and imaginary interactions, the radius and diffuseness of the matter distribution, and the folding parameter β_i of the imaginary potential.

For each angular distribution, the S matrix was extracted from ECIS and the near-side and far-side amplitudes were calculated with the method suggested by Fuller [4]. Whereas the total amplitude in the elastic scattering is given by

$$f = f_N + f_F = f_R + \frac{1}{2ik}\sum(2l+1)e^{2i\sigma_l}(S_l - 1)P_l(\cos\theta) , \tag{7}$$

where S_l denotes the S-matrix elements, σ_l the point Coulomb phase shifts, and $P_l(\cos\theta)$ the Legendre polynomials of first kind, the near-side (far-side) amplitude $f_{N(F)}$ is obtained from

$$f_{N(F)} = f_{R_{N(F)}} + \frac{1}{2ik}\sum(2l+1)e^{2i\sigma_l}(S_l - 1)Q_l^{(\mp)}(\cos\theta) . \tag{8}$$

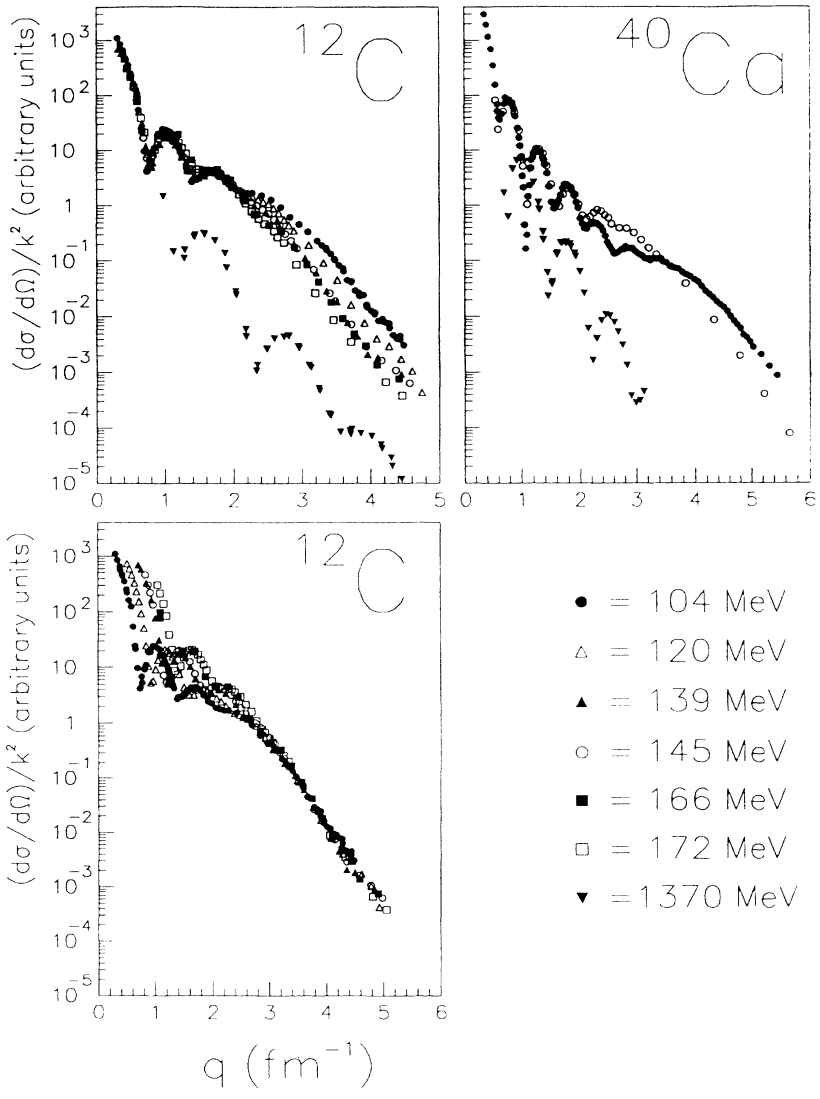

FIG. 1. Angular distributions for the differential cross sections divided by the squared wave number in the elastic scattering of alpha particles from ^{12}C and ^{40}Ca as a function of the momentum transfer q. In the lower set of curves for ^{12}C, the angular distributions have been arbitrarily shifted horizintally relative to the distribution obtained at 104 MeV.

Here f_{R_N} and f_{R_F} are the near-side and far-side Rutherford amplitudes [4] and $Q_l^{(\mp)}$ are linear combinations of Legendre functions of the first and second kinds according to

$$Q_l^{(\mp)}(\cos\theta)=\frac{1}{2}\left[P_l(\cos\theta)\pm i\frac{2}{\pi}Q_l(\cos\theta)\right] . \quad (9)$$

The experimental results we have analyzed are the Karlsruhe data [7] at 104 MeV, the Maryland data [8] at 140 MeV, and Orsay data [9] at 166 MeV, the Jülich data [10] at 120, 145, and 172.5 MeV, and the Saclay data [11] at 288, 340, 480, 699, and 1370 MeV. To get qualitatively similar data sets, some large angle scattering data have been excluded. Figure 1 shows the experimental data for ^{12}C and ^{40}Ca. In the upper part, the differential cross section data are divided by the squared wave number and are plotted versus the momentum transfer. If the nuclei had been "black disks," the angular distributions should have been identical. We observe that at the lower energies the diffractive region is similar and that the exponential falloff differs at large angles. The third plot below shows that the exponential falloff has about the same slope at all energies when the angular distributions are shifted in momentum transfer arbitrarily relative to the 104-MeV data. We will in Sec. III B show that these effects to a large extent are caused by the energy dependence of the real potential.

III. RESULTS AND DISCUSSION

Our calculations were rather extensive and we will only discuss some results in more detail. In Sec. III A we will describe the analyses for ^{58}Ni at 172.5 MeV. In Sec. III B we will study the energy dependence in the elastic scattering from ^{12}C in the energy region 104–1370 MeV and in Sec. III C the scattering from ^{58}Ni in the energy region 104–699 MeV. Finally, we will discuss some shortcomings of our simple folding model in Sec. III D.

A. Scattering from ^{58}Ni at 172.5 MeV

The results obtained for the elastic scattering of 172.5-MeV alpha particles from ^{58}Ni are found in Table I. The upper part was obtained with folding of both the real and imaginary potentials (f-f), whereas the lower part shows the results obtained with a Woods-Saxon parametrization for the imaginary potential (f-WS). As seen in Table I, nine different calculations were done with the value of the real folding parameter ranging from 0.0 to 2.5 fm.

Figure 2 shows the experimental data with the eight best fits with the real folding parameter ranging from 0.0 to 2.25 fm in the (f-f) case (upper set) and in the (f-WS) case (lower set). Even if the χ^2 values differ, all fits reproduce the main features of the angular distribution very well. In the (f-f) case, the angular distributions are almost indistinguishable up to 50°, and for larger angles there is just a modest difference in slope. The (f-f) set has a much smoother behavior, and this set gives thus an excellent opportunity to investigate the large-angle region in more detail and we will do such a study below.

We observe immediately in Table I that the two sets of data have systematic differences. The conventional assumption that the results for the real potential are not very sensitive to the shape of the imaginary potential is strongly questioned. The χ^2 values have a minimum for very large values of β_r when both potentials are folded. When the imaginary potential has a Woods-Saxon shape, the minimum χ^2 value is obtained for a very small value of β_r. This might be an indication that the real and imag-

TABLE I. Best fit parameters in the optical model calculations for the elastic scattering of 172.5-MeV alpha particles from ^{58}Ni. The upper sets have been obtained with both potentials folded; in the lower set the imaginary potential has a Woods-Saxon parametrization.

Real folding parameter	Matter density Reduced radius	Diffuseness a	Interaction Strength Real	Imaginary	α	β_i-β_r	χ^2	Mean square radii Matter distribution	Real potential	Imaginary potential	Volume integrals/nucleon Real potential	Imaginary potential
0.00	1.18	0.86	112.1	42.6	2.63	1.43	865	4.78	4.78	5.09	249.5	98.5
0.50	1.18	0.84	112.3	42.6	2.64	1.03	771	4.72	4.76	5.08	251.0	99.0
1.00	1.17	0.78	112.5	41.8	2.69	0.82	580	4.54	4.71	5.07	253.5	99.4
1.25	1.16	0.73	112.3	40.5	2.78	0.79	498	4.41	4.67	5.07	254.5	98.8
1.75	1.13	0.60	109.5	35.7	3.07	0.78	409	4.0	4.60	5.12	254.6	96.0
2.00	1.12	0.51	107.4	33.4	3.21	0.77	395	3.86	4.57	5.14	254.8	95.2
2.25	1.13	0.35	105.2	31.4	3.35	0.76	393	3.62	4.55	5.16	254.3	94.3
2.50	1.11	0.008	101.6	29.1	3.49	0.71	399	3.33	4.54	5.17	258.0	94.5
0.00	1.22	0.81	129.2	24.9	5.19		136	4.74	4.74	5.14	287.5	95.6
0.50	1.21	0.80	127.9	23.6	5.41		126	4.68	4.72	5.16	285.4	93.9
1.00	1.18	0.76	124.8	21.0	5.95		149	4.51	4.67	5.20	280.8	90.6
1.25	1.15	0.72	122.5	18.8	6.53		195	4.38	4.64	5.23	277.9	88.0
1.50	1.16	0.64	120.6	22.3	5.40		236	4.23	4.61	5.19	274.5	93.4
1.75	1.16	0.56	118.1	22.6	5.24		276	4.05	4.58	5.21	271.5	94.2
2.00	1.16	0.43	116.0	22.6	5.13		312	3.84	4.55	5.23	269.2	94.9
2.25	1.19	0.14	115.6	22.9	5.04		333	3.61	4.54	5.24	268.5	95.7
2.50	1.20	0.006	118.9	24.3	4.91		514	3.64	4.73	5.32	287.3	104.4

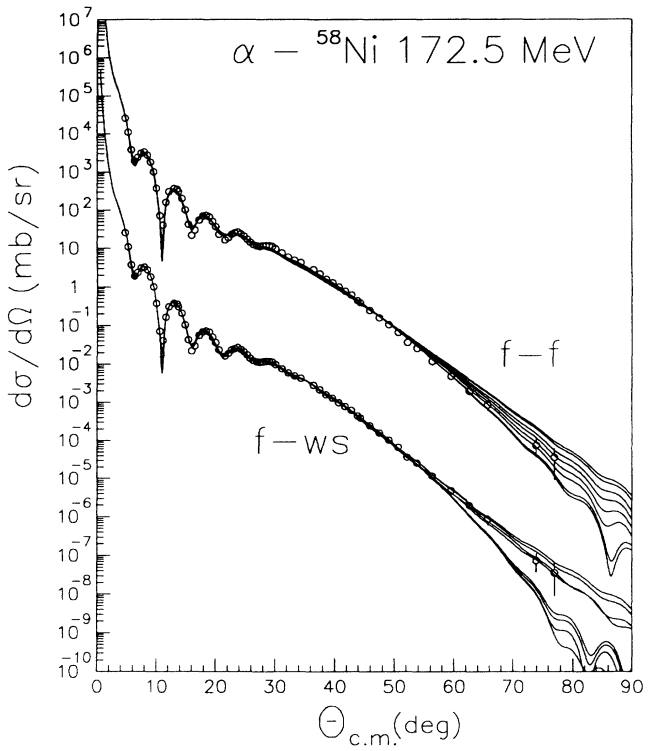

FIG. 2. Best fit angular distributions in the elastic scattering of 172.5-MeV alpha particles from ^{58}Ni. The upper set was obtained with both potentials folded. In the lower set, the imaginary potential has a Woods-Saxon shape.

inary potentials should have the same parametrizations. We also observe that the parameter which has the strongest correlation with β_r is the diffuseness a of the matter density. A more detailed study of all cases shows that for large values of β_r there is approximately a linear relation between the square of the diffuseness, a^2, and the real folding parameter β_r. From the first analysis of electron scattering, it is known that all nuclei should have a diffuseness of about 0.5 fm in a Woods-Saxon parametrization. Therefore too large values of β_r should be rejected even if they give lower χ^2 values. Consequently, the results in the figures will not include $\beta_r = 2.5$ fm.

Friedman *et al.* [12] have analyzed several nuclei at 104, 140, and 173 MeV using a Fourier-Bessel description of the optical potential. They quote the values of the volume integrals per nucleon for the real and imaginary potentials as 269±3 and 98 MeV fm^3 and for the rms radii 4.61±0.08 and 5.23 fm, respectively. Their results are in very good agreement with the (f-WS) results and in reasonable agreement with the (f-f) results in Table I. The consistency in the values of the volume integrals of the real and imaginary potentials and in the rms radii strongly supports the conclusion by Friedman *et al.* [12] that the folding model approach is appropriate for analyses of elastic scattering of alpha particles.

In heavy-ion scattering, it is well known that the real potentials, which reproduce the angular distribution for elastic scattering, tend to have the same value of the real potential at a specific radius. In an analysis of ^{12}C-^{12}C scattering [13], we found the same feature in Glauber calculations for a specific impact parameter. The invariant-sphere ambiguity was thus reduced to an invariant-circle ambiguity. It was therefore natural to look for similar phenomena in the elastic scattering of alpha particles, and we decided to plot all potentials as a function of r. We will also plot so-called "effective potentials." As shown by Wallace [14] and in Ref. [6], these potentials can be used in Glauber calculations and the results will then include the first-order noneikonal corrections. In the scattering of intermediate-energy alpha particles, the Glauber approximation with first-order noneikonal corrections does not reproduce a partial wave calculation very well [6]. The results are, however, much better with than without these corrections. Therefore the effective potentials should display the major effects of the imaginary potential on the effective refraction and of the real potential on the effective absorption. The effective potentials are given by

$$U_{\text{eff}}(r) = V(r) + \frac{1}{2kv}\left[2 + r\frac{d}{dr}\right]V(r)^2 , \tag{10}$$

where $V(r)$ is the sum of the optical and Coulomb potentials.

Figure 3(a) shows the matter densities in the (f-f) and (f-WS) cases. Figure 3(b) shows the nominal and effective real and imaginary potentials in the (f-f) case, and Fig. 3(c) shows those in the (f-WS) case. As seen, there is no indication of an invariant point in the real potential. For the imaginary potential, however, there is a weak indication for an invariant point at a very large r value. Instead, we observe first a remarkable and unexpected invariant point ambiguity in the matter distribution and, second, that the real potentials, nominal and effective, are extremely similar except very small radii in the (f-f) case. Since this invariant point in the matter density appeared for all nuclei in all energies, also with a Woods-Saxon parametrization of the imaginary potential, we decided to denote this radius as the *strong refraction radius* in analogy with the strong absorption radius. At first, we had the prefix Woods-Saxon Gaussian to indicate that this radius may be an effect of our parametrizations, but we found this too lengthy. The small uncertainty in the strong refraction radius in Fig. 3(a) is surprising with respect to the fact that we span such a large region for the folding parameter. We also note, however, a small difference between the strong refraction radii in the two cases. The most important feature of the strong refraction radius is of course that it is directly related to the matter density. The dashed curve in Fig. 3(a) shows the matter density for ^{58}Ni calculated by Fayans [15], and apparently the strong refraction radius has a reasonable value. A more detailed study of Table I for the f-f case shows that the rms radius for the real potential decreases by about 1% when the folding parameter is increased by 0.25 fm, whereas the variation in the volume integral is considerably smaller. The strong refraction might thus be due to the fact that the volume integral of the real potential is constant. In the f-WS case, however, both the rms radius and the volume integral decrease with increasing

folding parameter, and so there is no obvious explanation to the strong refraction radius.

Several authors have done so called "notch tests" of the real potentials in order to investigate the radial sensitivity of the elastic scattering of alpha particles. In these tests, parts of the optical potential are removed artificially. Our results indicate that in folding model calculations such tests might be much more interesting for the matter density.

Figure 4 shows the result of a near-side and far-side decomposition of the angular distributions shown in Fig. 2. The solid curve shows the total cross section, whereas the dashed and dotted curves show the near-side and far-side cross sections. As seen, the interference between the two components results in a diffractive pattern for small angles. For the angular region 30°–80°, the far-side amplitude is so dominating that the total cross section essentially is identical with the far-side cross section. As shown by Hussein and McVoy [3], this asymmetry is an effect of the refraction in presence of absorption. McVoy and Satchler [16] have discussed the possibility to observe nuclear rainbows in the elastic scattering of heavy ions.

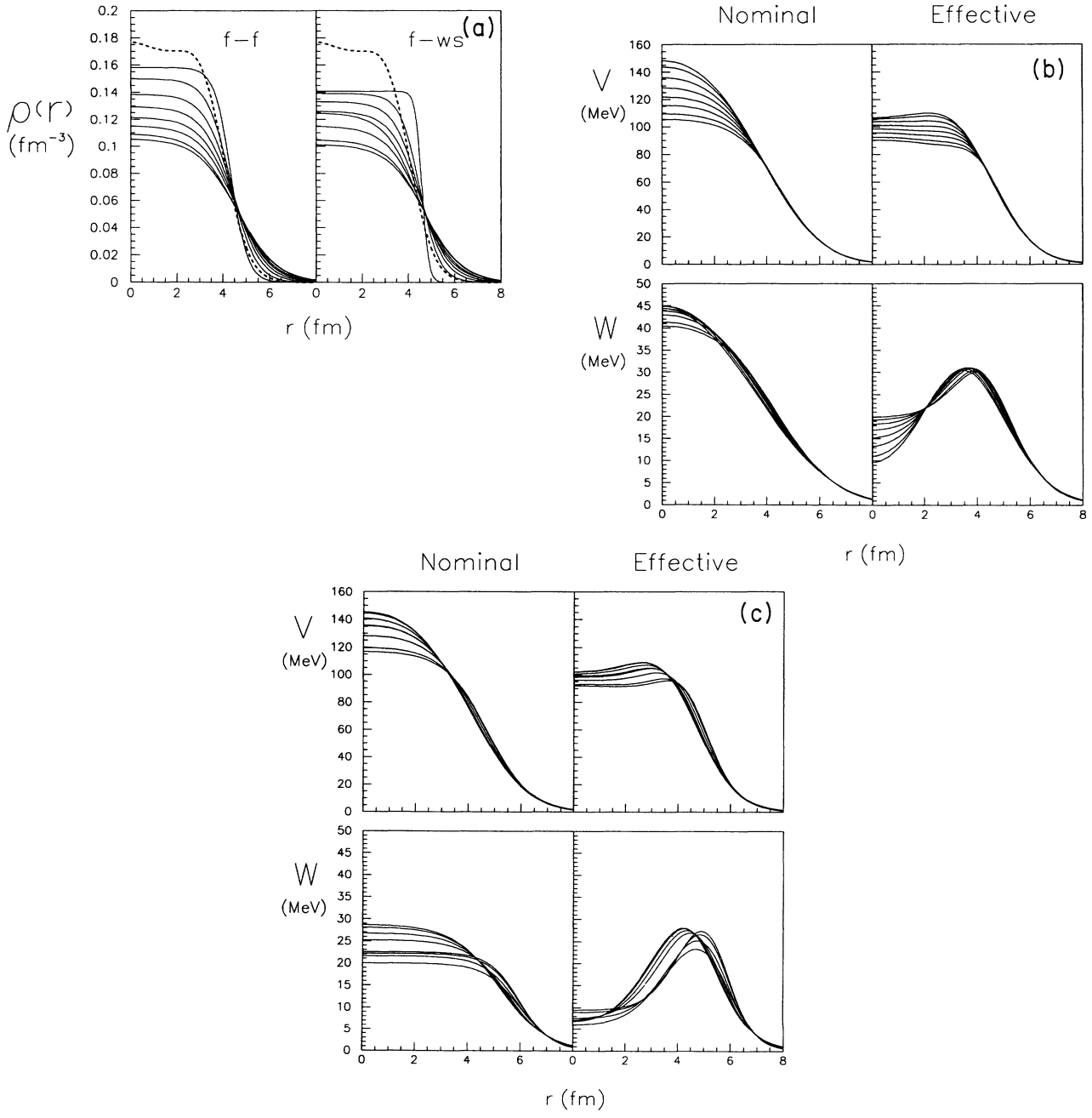

FIG. 3. Results obtained with both potentials folded (f-f) and with the real potential folded and the imaginary one of the Woods-Saxon shape. (a) shows the matter densities in the two cases. The dashed curve shows the matter density for ^{58}Ni, calculated by Fayans [15]. (b) and (c) show the nominal and effective potentials, as described in the text, in the (f-f) and (f-WS) cases, respectively.

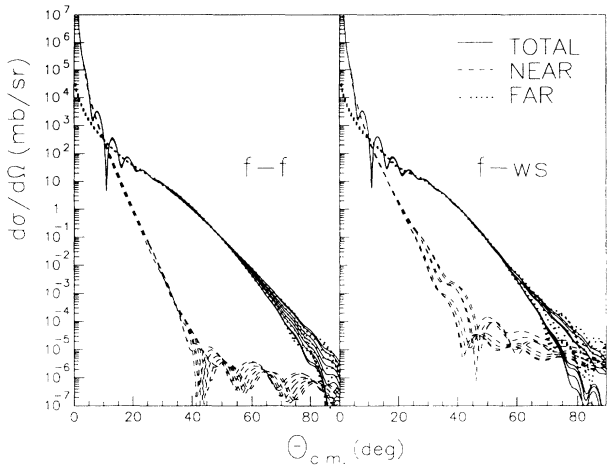

FIG. 4. Total, near-side, and far-side differential cross sections for the two cases shown in Fig. 2.

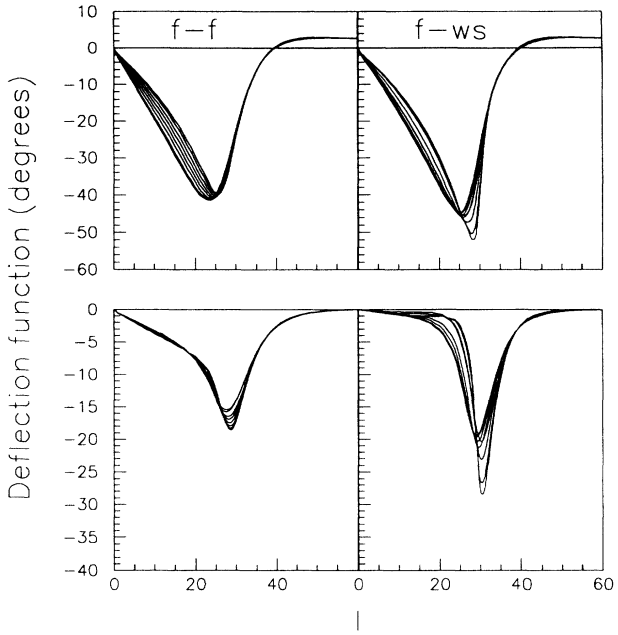

FIG. 5. Real (upper part) and imaginary (lower part) parts of the deflection functions for the two cases shown in Fig. 2.

They start their discussion from the nuclear deflection function θ_l, defined as the real part of $2\partial\delta_l/\partial l$, where δ_l is the sum of the nuclear and Coulomb phase shifts. From the minimum in the real deflection function, they define the rainbow scattering angle Θ_R, in analogy with classical scattering theory. The angular region inside Θ_R is called the bright side and the region outside is called the dark side. The cross section on the dark side arises in the semiclassical interpretation from a single complex L value so that $d\sigma/d\theta \propto \exp[-(\mathrm{Im}L)\theta]$. This explains the exponential falloff for the differential cross section on the dark side. On the bright side each angle Θ can be reached by two L values, $L_<$ and $L_>$. The interference between these two contributions produces broad Airy maxima, separated with $\Delta\Theta \approx 2\pi/(L_> - L_<)$. McVoy and Satchler emphasize that the last semiclassical conclusion does not consider the fact that the contribution from the smaller L value, $L_<$, will be much more damped by the presence of the imaginary potential.

We calculated the real as well as the imaginary part of the deflection functions to get a more detailed comparison between the potentials. The results obtained in the f-f and f-WS cases are shown in the left and right sides of Fig. 5. The upper and lower parts show the real and imaginary parts, respectively. The rainbow angle appears for $l \approx 25$ and varies between 39° and 42° in the f-f case and between 45° and 52° in the f-WS case. We also observe that the angular distributions in Fig. 2 essentially only differ on the dark side. To investigate to what extent the slope of the exponential falloff is a pure refractive effect, we performed two further calculations. In the first one, shown in the left part of Fig. 6, the calculations were performed with the real potential obtained with $\beta_r = 1.50$ fm, and the imaginary potentials obtained with $\beta_r = 1.00$, 1.25, 1.50, 1.75, and 2.00 fm. In the set to the right, the calculations were done with the imaginary potential obtained with $\beta_r = 1.50$ fm and the real potential was varied in the same way. As seen, both sets of curves are unaffected at small angles. The change when the imaginary potential is varied may be interpreted as a damping of the amplitude or an angular displacement of the exponential falloff. When the real potential varies, it is just the slope on the dark side that changes. If we now study the real potential in Fig. 3(b) again, it is obvious that the slope of the exponential falloff is determined by the behavior of the real potential inside 4 fm. If we study the deflection functions in Fig. 5, it is difficult to judge to what extent the slope is determined by the l value of the rainbow angle and to the behavior for small l values. Since the bright side differential cross sections do not

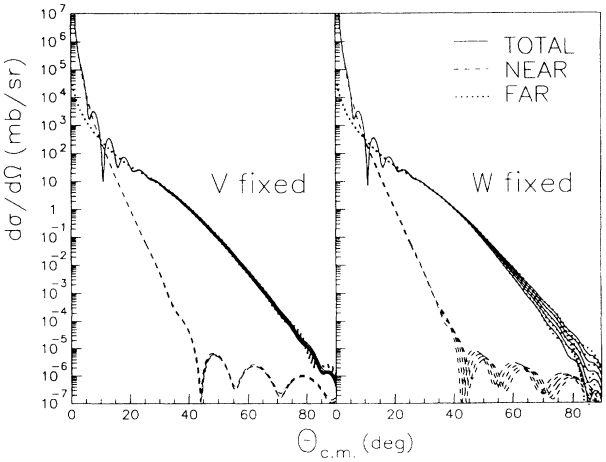

FIG. 6. Angular distributions calculated with the real potential obtained from the fitting procedure in the (f-f) case with $\beta_r = 1.50$ and the imaginary potentials from the fitting procedures with $\beta_r = 1.00$, 1.25, 1.50, 1.75, and 2.00 (left part). In the right part, the imaginary potential was fixed at the value obtained with $\beta_r = 1.50$ and the real potential was varied in the same way.

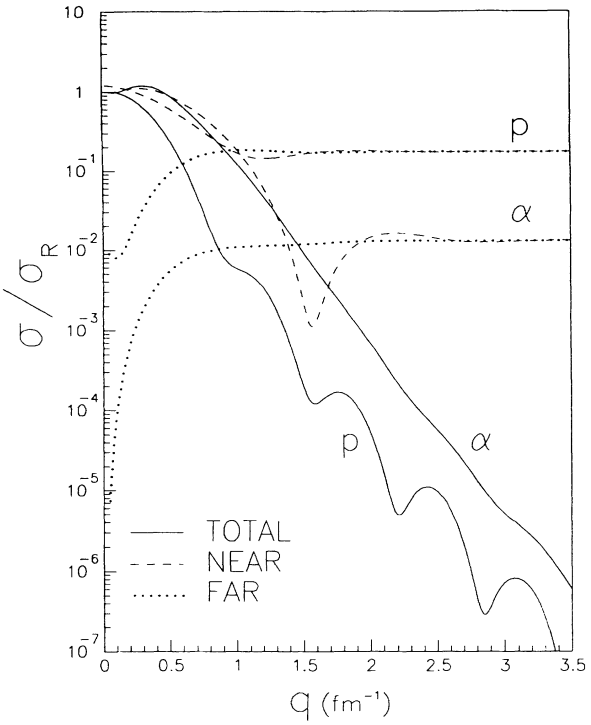

FIG. 7. Angular distributions for the differential cross section divided by the Rutherford cross section for 172.5-MeV alpha particles and protons scattered from an extended charge distribution in ^{58}Ni without any nuclear interaction.

differ, we observe no dependence on the l value, $L_<$, discussed above and therefore we will not further discuss the possibility of observing a nuclear rainbow in the angular distribution.

The results obtained indicate that more accurate data for large angles should make it possible to determine the interior of the optical potential in a much more unambiguous way.

It is of interest to remark in this context that also the form factor in pure Coulomb scattering for 172.5-MeV alpha particles shows a structureless falloff [6]. Figure 7 shows the differential cross section divided by the Rutherford cross section as a function of the momentum transfer for alpha particles and protons at the same energy. As seen, the near-side and far-side cross sections are much larger for protons, but they interfere much more destructively and show a diffractive pattern with indication of a radius for the charge distribution. The structureless total cross section for alpha particles is much closer to the Rutherford point cross section, though the phase shifts are much larger and many more. We believe that this effect is caused by the rapid variation of the phase shifts in the nuclear surface for alpha particles.

B. Scattering from ^{12}C in the energy region 104–1370 MeV

In the case of ^{12}C, we analyzed data at 104, 120, 139, 145, 166, 172, and 1370 MeV. The differential cross sections, together with the near-side and far-side cross sections, are shown, together with the experimental results in Fig. 8 for 104, 120, 145, 172, and 1370 MeV. One observes that the experimental results are satisfactorily reproduced, and the total cross section is very similar to the farside cross section except for small and very large angles and at 1370 MeV. It is also evident that the asymmetry between the near-side and far-side cross sections decreases with increasing energy and is very small at 1370 MeV, where the angular distribution has a typical diffractive pattern. The deflection functions are shown in Fig. 9 as a function of l/k. As seen with varying energy, they vary in shape as well as in magnitude. If one determines the rainbow angle from the minimum of the real deflection function, one can calculate the momentum transfer at this angle. From Fig. 9 we found that the rainbow angle was shifted relative to the one at 104 MeV with 0.18, 0.62, and 1.00 fm^{-1} at 120, 145, and 172 MeV, respectively. Compared to the arbitrary shifts in q used

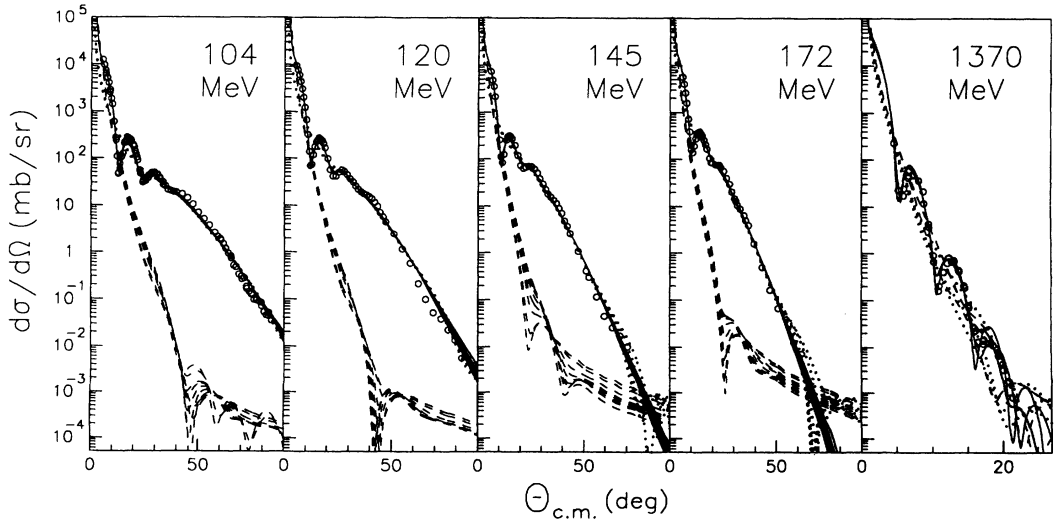

FIG. 8. Angular distributions for the total, near-side, and far-side differential cross sections in the elastic scattering from ^{12}C at 104, 120, 145, 172, and 1370 MeV.

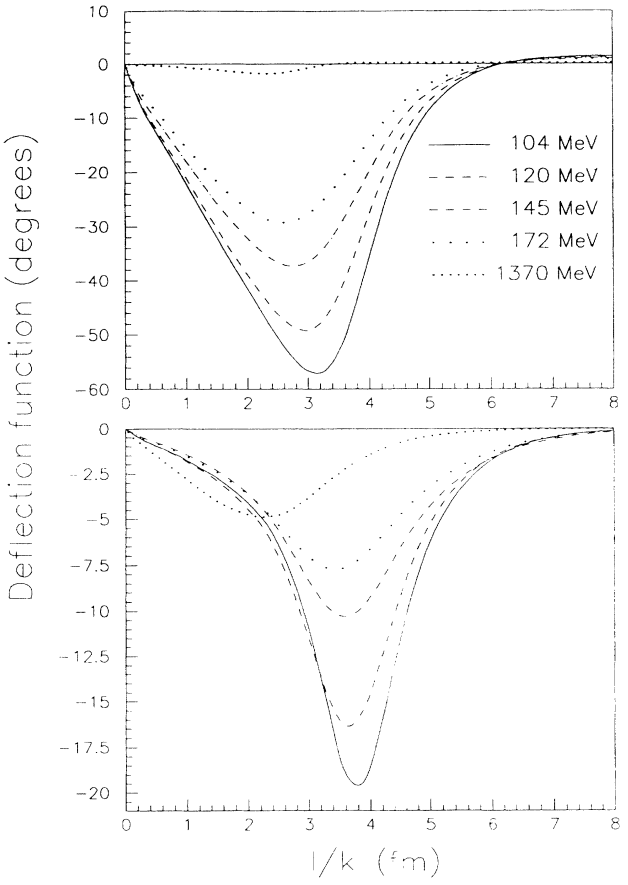

FIG. 9. Real (upper part) and imaginary (lower part) parts of the deflection functions as a function of l/k for the cases shown in Fig. 8.

in the lower part of Fig. 1, i.e., 0.18, 0.42, and 0.60 fm^{-1}, the rainbow shifts are somewhat larger. It is of interest to note that the different curves in the lower part of Fig. 1 start to coincide close to the momentum transfer for the rainbow angle at 104 MeV, corresponding to a momentum transfer of 3.2 fm^{-1}.

The matter densities obtained in the five cases are shown in Fig. 10. In all cases there is a well-defined strong refraction radius which agrees well with the matter density. In this case the matter density was calculated from Sick's charge density [17] assuming equal densities for protons and neutrons.

As discussed by Hussein and McVoy [3], the Coulomb interaction does not change the slope of the exponential falloff, but merely causes a shift in angle. Since the strength of the nuclear potential varies relatively the nuclear potential with energy, we decided to investigate whether the Coulomb interaction to some extent could explain the angular shifts between the angular distributions shown in Fig. 1. It turned out, however, that this effect was almost negligible. Instead, we decided to perform a calculation with the potential obtained with $\beta_r = 1.50$ fm for 104 MeV and only vary the strength of the real potential. The results obtained for the total and near-side cross sections are found in Fig. 11. The solid curves show the result with the full potential. The dashed curves were obtained with 18%, the dot-dashed curves with 50%, and the dotted curves with 75% reduction of the real potential. The 18% reduction was obtained from the ratio between the volume integrals obtained at 104 and 172 MeV. It is striking how well the curves reproduce the gross features of the energy dependence shown in Fig. 1. The 18% reduction has a very small effect on the diffractive part and it reproduces very well the difference between the experimental results at

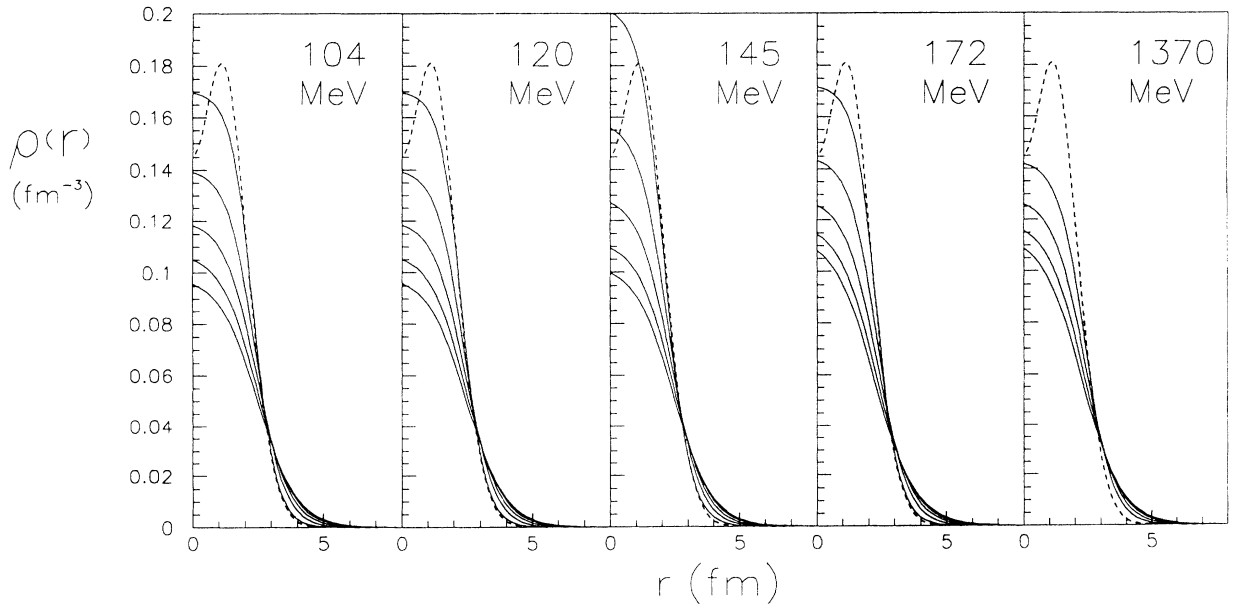

FIG. 10. Best fit matter densities for ^{12}C obtained with the values 1.00, 1.25, 1.50, 1.75, and 2.00 at the lower energies and 0.00, 0.50, and 1.00 at 1370 MeV for the real folding parameter β_r. The dashed curve shows the matter density obtained from Sick's charge density for ^{12}C [17].

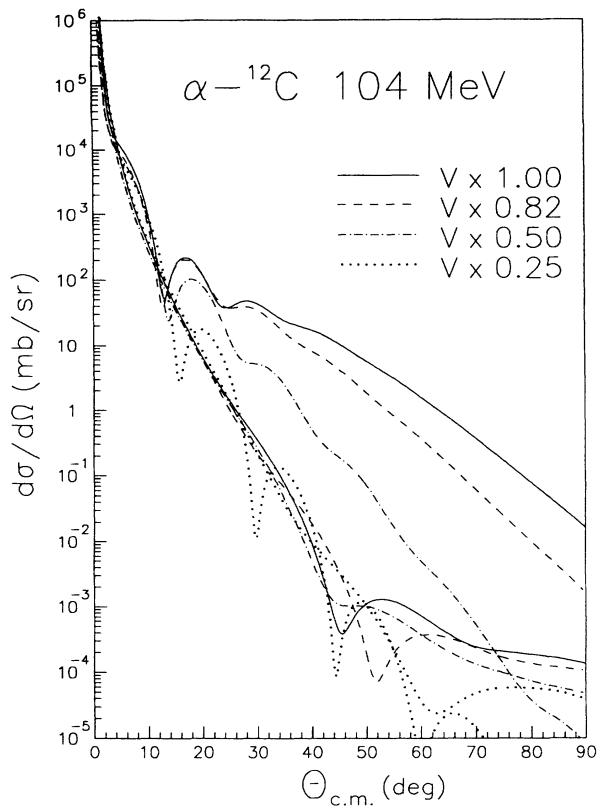

FIG. 11. Total and near-side cross sections (with the same notation) in the elastic scattering from ^{12}C at 104 MeV with different strengths of the real potential.

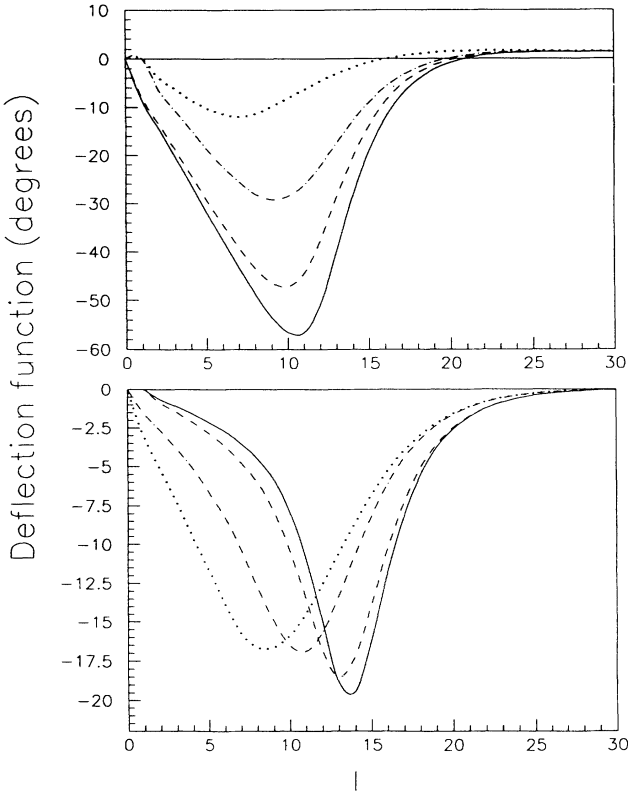

FIG. 12. Deflection functions for the calculations shown in Fig. 11.

104 and 172 MeV. Also, the arbitrarily chosen 75% reduction gives a result very similar to the one obtained at 1370 MeV. It is of interest to note that the near-side cross section is very insensitive to the strength of the real potential up to about 40° and that when the refractive effects become small the total cross section oscillates around the near-side cross section.

The deflection functions for these four different strengths of the real potential are shown in Fig. 12. Regarding the real part, we observe not only a decrease in the rainbow angle, but also a decrease in the l value for which it appears. The effects on the imaginary part are very dramatic, in spite of the fact that the imaginary potential is the same. Our results confirm the results of Ref. [2], and we observe how the real potential increases the imaginary phase shifts in the surface, which in turn increases the strong absorption radius, but also decreases the absorption for small partial waves.

The deflection functions obtained by varying only the strength of the real potential are of course not very realistic, as can be seen from a comparison with Fig. 9. Such a variation reproduces, however, the gross features of the angular distributions in a surprisingly realistic way. The strong effects of the real potential on the absorption clearly call into doubt a semiclassical interpretation of the angular distributions.

In comparisons between heavy-ion and alpha particle scattering it has been found that the differential cross sections for heavy ions are comparatively small and one has introduced the concept of surface transparency. We think that this term is rather misleading, and a more realistic concept should be *refractive surface absorption.* It should be stressed that the increased absorption in the surface is combined with a decreased absorption for small partial waves, and as a result of the strong refraction, the alpha particle can probe the interior of the nucleus.

Finally, we want to stress the extremely large effects of refraction that are present in scattering of alpha particles. Figure 11 shows that the differential cross section should be reduced with more than a factor of 1000 in a large angular range if the real potential had been small. It is also remarkable of course that this increase comes only from the far-side cross section.

C. Scattering from ^{58}Ni in the energy region 104–699 MeV

At last, we describe in detail our results for ^{58}Ni. The reason for this choice is the fact that ^{58}Ni is one of the few nuclei for which the elastic scattering has been measured above 172 MeV. Figure 13 shows a near-side and far-side decomposition of the angular distributions obtained at 104, 288, 340, 480, and 699 MeV, as a complement to the results at 172.5 MeV, shown in Fig. 4. The calculations shown in Fig. 13 were performed with conventional Woods-Saxon potentials. Since the absorption is more dominant for a heavier nucleus, the diffractive re-

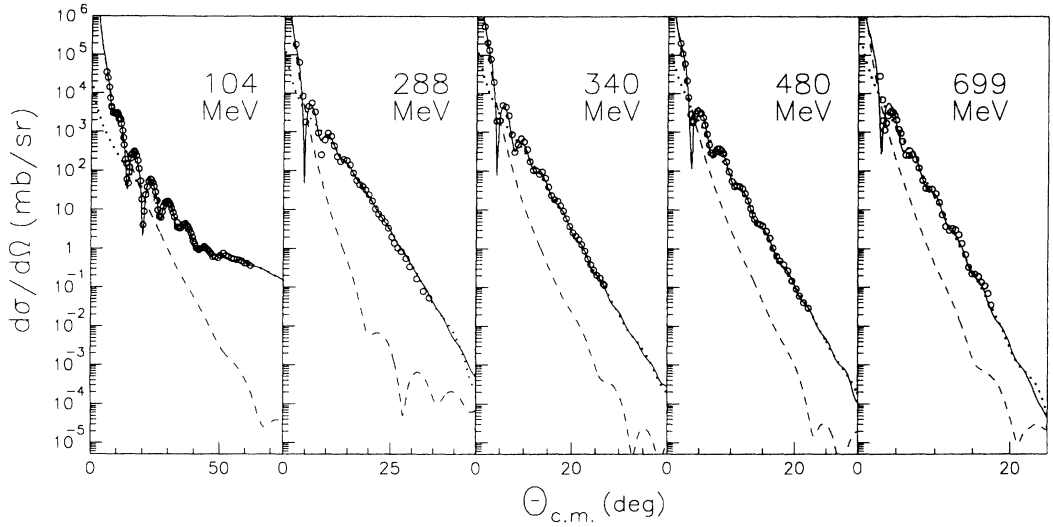

FIG. 13. Angular distributions for the total, near-side, and far-side differential cross sections in the elastic scattering from ^{58}Ni at 104, 288, 340, 480, and 699 MeV.

gion is more extended for ^{58}Ni than it was for ^{12}C. The effects of the refraction is, however, very important also in this case. The refractive effects decrease slowly with energy, but also at 699 MeV the ratio between the far-side and near-side cross sections is as large as a factor of 10 in a large angular region.

D. Dependence on atomic number and energy in the folding calculations

The results obtained for different nuclei at different energies are rather consistent for the volume integrals of the potentials. We have also a clear indication that the folding parameter should be larger for the imaginary potential than for the real one. This is exemplified in Table II with the values obtained at 104 and 140 MeV. The results for ^{208}Pb deviate somewhat. We also note that some variations seem to be correlated to the difference in the folding parameters. From this we learn that in a future calculation the imaginary folding parameter should be larger than the real one. The difference should not vary, however, if one wants to extract reliable values for the strength of the interaction.

The major problem with our results is the total diffuseness, i.e., the relation between the diffuseness of the matter density, a, and the real folding parameter β_r. As mentioned above, a good fit was found to require that $a^2+\text{const}\times\beta_r$ have the same value. The constant was found to be of the order of 0.3 and varied somewhat from case to case. This expression could thus be considered as an "effective diffuseness" in the alpha-nucleus interaction. Figure 14 shows the values of a^2 plotted versus β_r for the nuclei studied at 104 and 140 MeV. One observes that for the same value of β_r the diffuseness seems to increase strongly with the atomic number. We interpret this as a strong indication of a density dependence in the interaction. It has been shown [1] that with a density dependence it is possible to get better agreement with the experimental results and that the main effect is to make the potential weaker for small r values. We argue, however, that the density dependence is required to make the surface more diffuse.

The values of the folding parameter seem to decrease with energy. At 1370 MeV the folding parameters are very small, in the case of ^{12}C as well as ^{40}Ca. The diffuseness goes negative for $\beta_r=1.50$. Such small folding parameters are of course unrealistic, and it is difficult to believe that a density dependence could drastically change this result for such a light nucleus as ^{12}C. We

TABLE II. Best fit parameters obtained in the analyses of the elastic scattering of alpha particles of 104 and 140 MeV. The five values at each position have been obtained with the values 1.00, 1.25, 1.50, 1.75, and 2.00 fm for the real folding parameter β_r.

Energy (MeV)	Nucleus	Volume integrals/nucleon Real potential					Imaginary paotential					β_i-β_r (fm)				
104	^{12}C	321	321	321	321	344	106	107	107	107	107	0.77	0.66	0.57	0.50	0.45
	^{40}Ca	302	300	298	295	293	116	113	111	108	106	0.93	0.91	0.91	0.91	0.89
	^{48}Ca	313	309	306	304	294	115	114	112	110	105	0.97	0.96	0.93	0.92	0.93
	^{58}Ni	301	297	291	292	292	163	149	135	138	140	0.01	0.14	0.28	0.25	0.17
	^{208}Pb	342	360	365	359	346	107	98	84	90	84	1.23	1.35	1.75	1.47	1.68
140	^{12}C	273	274	277	278	278	107	108	109	109	109	0.92	0.79	0.67	0.59	0.53
	^{40}Ca	278	279	279	280	281	117	115	113	110	110	0.68	0.67	0.66	0.66	0.62
	^{208}Pb	377	373	371			77	75	75			1.25	1.27	2.12		

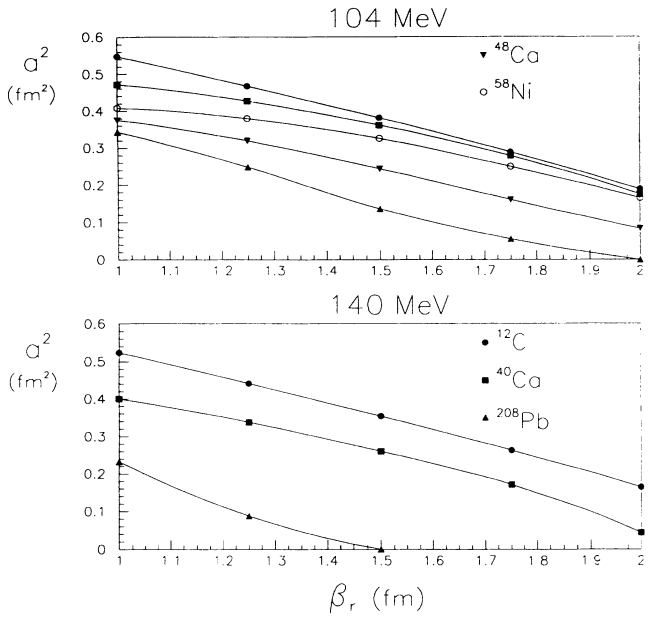

FIG. 14. Square of the best fit diffuseness a^2 plotted versus the real folding parameter β_r at 104 and 140 MeV. The curves are drawn as guides for the eye.

have become rather convinced that the scattering of alpha particles at this energy must be performed with a relativistic potential. In such a calculation, the optical potential is the sum of a scalar and vector potential and this sum can of course give a potential with a much sharper surface if the two potentials have different shapes.

Regarding all problems with dependence on atomic number and energy, it is quite remarkable that in all cases studied we have found a well-defined strong refraction radius also at 1370 MeV where the folding parameter has unreasonably small values.

IV. CONCLUSIONS

The goal of our calculations reported here was to learn more about the energy dependence of the effective alpha-nucleon interaction as a preparation for the analysis of total reaction cross sections, which we plan to measure at The Svedberg Laboratory in Uppsala in the energy range 100–200 MeV. We have learnt that the gross features of the energy dependence of the angular distributions is due to the energy dependence in the real potential. The refraction affects mainly the far-side contribution and increases the total cross section by several orders of magnitude in a large angular region.

The very strong interaction of alpha particles has the effect of producing a strong interference between refractive and absorptive effects. The refraction increases the imaginary phase shifts for large l values so that the strong refraction radius increases considerably. We denote this effect as refractive surface absorption. For small partial waves, however, the absorption decreases with increasing refraction, and thus the possibility to extract information from small radii is improved.

Our results show that our planned measurements of total reaction cross sections will make it possible to determine not only the imaginary, but also the real potential with greater accuracy.

ACKNOWLEDGMENTS

We wish to thank K. McVoy for the program for the decomposition of the Rutherford amplitude into near-side and far-side amplitudes and S. A. Fayans for the matter density for ^{58}Ni. We want to thank H. J. Gils and S. Wiktor for providing us with some of the data analyzed here. We also wish to thank G. Fäldt for critical comments on the manuscript.

[1] C. J. Batty, E. Friedman, H. J. Gils, and H. Rebel, Adv. Nucl. Phys. **19**, 1 (1990).
[2] A. Ingemarsson and G. Fäldt, Phys. Rev. C **48**, 507 (1993).
[3] M. S. Hussein and K. W. McVoy, Prog. Part. Nucl. Phys. **12**, 103 (1984).
[4] R. C. Fuller, Phys. Rev. C **12**, 1561 (1975).
[5] J. Raynal, IAEA, Vienna, Report No. IAEA-SMR9/8 281, 1972; IAEA, Vienna, Report No. IAEA-SMR8/8 75, 1972.
[6] G. Fäldt and A. Ingemarsson, Phys. Rev. C **46**, 1974 (1992).
[7] H. J. Gils, E. Friedman, H. Rebel, J. Buschmann, S. Zagromski, H. Klewe-Nebenius, B. Newmann, R. Pegl, and G. Bechtold Phys. Rev. C **21**, 1239 (1980); Kernforschungszentrum, Karlsruhe, Internal Report No. KfK-2838, 1979; H. J. Gils, Kernforschungszentrum, Karlsruhe, Internal Report No. KfK-3765, 1984; H. J. Gils, H. Rebel, and E. Friedman, Kernforschungszentrum, Karlsruhe, Internal Report No. KfK-3556, 1983; Phys. Rev. C **29**, 1295 (1984); H. J. Gils, Kernforschungszentrum, Karlsruhe, Internal Report No. KfK-2225, 1975; H. J. Gils, E. Friedman, Z. Majka, and H. Rebel, Phys. Rev. C **21**, 1245 (1980; G. Schatz *et al.*, Nucl. Phys. **A128**, 81 (1969); H. J. Gils and H. Rebel, Z. Phys. A **274**, 279 (1975); H. J. Gils *et al., ibid.* **279**, 55 (1976); V. Corcalciuc, H. Rebel, R. Pesl, and H. J. Gils, J. Phys. G **9**, 177 (1983).
[8] D. A. Goldberg, S. M. Smith, and G. F. Burdzik, Phys. Rev. C **10**, 1362 (1974); P. L. Roberson, D. A. Goldberg, N. S. Wall, L. W. Woo, and H. L. Chen, Phys. Rev. Lett. **42**, 54 (1979); D. A. Goldberg, S. M. Smith, H. G. Pugh, P. G. Roos, and N. S. Wall, Phys. Rev. C **7**, 1938 (1973).
[9] B. Tatischeff and I. Brissaud, Nucl. Phys. **A155**, 89 (1970).
[10] S. Wiktor, Mayerbor, A. Kiss, M. Rogge, P. Turek, and H. Dabrowski, Acta Phys. Pol. B **12**, 491 (1981); J. Albinski, A. Budzanowski, H. Dabrowski, Z. Rogalska, and S.

Wiktor, Nucl. Phys. **A445**, 367 (1985); A. Kiss, C. Mayerbor, M. Rogge, P. Turek, and S. Wiktor, J. Phys. G **13**, 1067 (1987).
[11] A. Chauemaux, Nucl. Phys. **A267**, 413 (1976); G. Alkhazov *et al., ibid.* **A280**, 365 (1977); B. Bonin, N. Alamanos, B. Berthier, G. Bruge, H. Faraggi, J. C. Lugol, W. Mittig, L. Papineau, and A. I. Yavin, *ibid.* **A445**, 381 (1985).
[12] E. Friedman, H. J. Gils, H. Rebel, and R. Pesl, Nucl. Phys. **A363**, 137 (1981).
[13] G. Fäldt and A. Ingemarsson, Phys. Scr. **28**, 454 (1983).
[14] S. J. Wallace, Ann. Phys. (N.Y.) **78**, 190 (1973).
[15] S. A. Fayans (private communication).
[16] K. W. McVoy and G. R. Satchler, Nucl. Phys. **A417**, 157 (1984).
[17] I. Sick, Nucl. Phys. **A218**, 509 (1974).